九州大学学術情報リポジトリ
Kyushu University Institutional Repository

Synthesis of platinum silicide at platinum/silicon oxide interface by photon irradiation

Sato, K.
Research Center for Ultra-High Voltage Electron Microscopy, Osaka University

Yasuda, H.
Research Center for Ultra-High Voltage Electron Microscopy, Osaka University

Ichikawa, S.
Research Center for Ultra-High Voltage Electron Microscopy, Osaka University

Imamura, M.
Synchrotron Light Application Center, Saga University

他

https://hdl.handle.net/2324/7393039

出版情報：Acta Materialia. 154, pp.284-294, 2018-08-01. Elsevier
バージョン：
権利関係：Creative Commons Attribution-NonCommercial-NoDerivatives 4.0 International

KYUSHU UNIVERSITY

Synthesis of platinum silicide at platinum/silicon oxide interface by photon irradiation

K. Sato,[a,b,*] H. Yasuda,[a,b] S. Ichikawa,[a] M. Imamura,[c] K. Takahashi,[c] S. Hata,[d,e] S. Matsumura,[d,f] S. Anada,[g] J.-G. Lee,[h] and H. Mori[a]

[a]*Research Center for Ultra-High Voltage Electron Microscopy, Osaka University, Ibaraki, Osaka 567-0047, Japan*

[b]*Division of Materials and Manufacturing Science, Graduate School of Engineering, Osaka University, Suita, Osaka 565-0871, Japan*

[c]*Synchrotron Light Application Center, Saga University, Honjo 1, Saga 840-8502, Japan*

[d]*The Ultramicroscopy Research Center, Kyushu University, Motooka, Fukuoka 819-0395, Japan*

[e]*Department of Advanced Materials Science and Engineering, 6-1 Kasugakoen, Kasuga-shi, Fukuoka 816-8580, Japan*

[f]*Department of Applied Quantum Physics and Nuclear Engineering, Kyushu University, Motooka, Fukuoka 819-0395, Japan*

[g]*Japan Fine Ceramics Center, Nanostructures Research Laboratory, Mutsuno, Atsuta, Nagoya 456-8587, Japan*

[h]*Powder & Ceramics Division, Korea Institute of Materials Science, Changwon, Gyeongnam 642-831, Korea*

*Corresponding author. Tel.: +81 (0)6 6879 7941; fax. +81 (0)6 6879 7942

E-mail: sato@uhvem.osaka-u.ac.jp (K.S.)

Abstract

The synthesis of platinum silicide at a Pt/SiO_x interface by photon irradiation was investigated using transmission electron microscopy. A platinum silicide, Pt_2Si, was successfully formed at the Pt/SiO_x interface by irradiation with 680 and 140 eV photons, but not by irradiation with 80 eV photons. Silicide formation was also induced by irradiation with electrons of energy 75 keV. The amount of silicide formed by photon irradiation was lower than the amount obtained by electron irradiation. Silicide formation by both photon and electron irradiation was accompanied by Si depletion in amorphous SiO_x. The experimental results indicate that silicide formation is induced by electronic excitation. A possible mechanism for silicide formation is proposed on the basis of the results.

Keywords: Transition-metal silicide; Synchrotron radiation; Transmission electron microscopy; Electronic band structure; Electronic excitation

1. Introduction

High-energy particle irradiation (i.e., ion and electron irradiation) is widely used and is one of the most effective tools for materials modification. Studies of this subject are of significance not only from the scientific point of view, for elucidation of the mechanisms behind the modifications, but also from the technological point of view, to achieve advanced functionalization of materials. If we confine ourselves to inorganic nonmetallic materials, examples of studies in this area are as follows: formation of amorphous Si with a controlled degree of crystallinity by co-irradiation with MeV electrons and MeV ions [1], recoil implantation of foreign atoms into semiconducting substrates by MeV electron irradiation [2], amorphization of crystalline Si by MeV electron irradiation [3], doping of impurity atoms into semiconductors by ion implantation [4], and defect formation in CeO_2 by irradiation with a few hundred MeV ions [5,6].

In general, materials modification by high-energy particle irradiation can be achieved by two different routes, namely atom displacement caused by the direct knock-on of primary particles, and processes caused by excitation of the electronic system. (The latter includes, in some cases, atom migration and/or atom displacement, in addition to modification of electronic states.) However, our understanding of electronic excitation effects in materials modification is still insufficient, in contrast to the current, deeper understanding of knock-on atom displacement. At present, it is therefore difficult to investigate the two contributions separately in detail. Consequently, it is of primary importance to improve our understanding of the effects of electronic excitation on materials modification.

In view of this background, research on whether or not a solid-state reaction can be controlled by excitation of the electronic system can be regarded as one of the most

interesting research themes that touch the core of this subject. On the basis of this premise, two of the present authors (HY and HM) have been engaged in the study of solid-state reactions that do not occur under thermal annealing conditions (i.e., solid-state reactions for which the Gibbs free energy change, ΔG, is positive) but do occur in an electron excitation environment [7, 8], with a focus on reactions induced by excitation of inner-shell electrons. To date, it has been found that (1) a compound semiconductor, GaSb, can be decomposed or dissociated to a mixture of Ga and Sb by low-energy electron irradiation, with no knock-on atom displacement [7], although ΔG for the decomposition reaction, GaSb(s) → Ga(s) + Sb(s), is positive, and that (2) a silicide, Pt_2Si, can be successfully synthesized at the Pt/SiO_x interface by similar electron irradiation [8], although ΔG for the silicide synthesis reaction is again positive [9]. Experimental results for silicide synthesis [8] suggest that dissociation of the substrate material, SiO_x, is first induced by electronic excitation and then one of the dissociation products (i.e., a Si atom) may react with neighboring Pt deposited on the substrate, resulting in the formation of a Pt_2Si layer at the Pt/SiO_x interface. Photochemical research on isolated molecules has established that there are examples of synthesis reactions in which fragmental species (mainly constituent atoms) produced by photoinduced dissociation reactions serve as one of the starting materials (or starting components) for the subsequent synthesis reaction [10]. However, to the best of our knowledge, no such examples have been reported in the field of solid-state reactions of inorganic materials.

It is therefore of interest to study whether or not the dissociation product (i.e., Si atoms) from the SiO_x substrate can actually serve as a starting material (or starting component) and participate in the subsequent reaction with the pre-existing Pt, eventually leading to silicide synthesis, using Pt/SiO_x composite samples. In the present study, to

elucidate the mechanism behind the synthesis reaction, we used electromagnetic radiation (i.e., photon irradiation), with which energy-selective excitation of electrons can be achieved more accurately than with conventional electron irradiation, as, for example, in transmission electron microscopy. Based on these considerations, in this work, the synthesis of platinum silicide at the Pt/SiO_x interface, induced solely by photon irradiation, was investigated. The results confirmed that a silicide, Pt_2Si, can be successfully formed at the Pt/SiO_x interface by photon irradiation.

The authors believe that this work provides information that will contribute to a better understanding of electronic excitation effects in materials modification.

2. Experimental Procedures

2.1. Sample preparation

Samples were prepared by two different methods. In the first method, Pt particles were grown almost epitaxially on (001)-cleaved NaCl substrates, kept at 573 K, by DC sputtering of a Pt target in a high-purity argon plasma (5N purity). The argon pressure in operating mode was 8 Pa, and the applied voltage and duration were 370 V and 30–50 s, respectively. The particles were then backed with a supporting film, namely an amorphous SiO_x film of thickness approximately 20 nm, which was vapor deposited onto the Pt particles on the NaCl, after it had been cooled to room temperature. Lumps of silicon monoxide were used as the source. In the composite, Pt particles were embedded in one side of an amorphous SiO_x film [see Fig. S3(a) in the supplementary material (SM) for reference [8]], and Pt particles showed a strong preferred orientation along the [001] direction because of the epitaxial growth mentioned above. In the other method, amorphous SiO_x films of thickness approximately 20 nm were formed by vapor

deposition on (001)-cleaved NaCl substrates kept at room temperature. Then Pt particles of size ~10 nm were formed on the oxide film at room temperature by DC sputtering of a Pt target under conditions similar to those used in the first method. The duration period was about 15 s. The orientation of grains in individual Pt particles was random, as can be seen from the continuous Debye–Scherrer rings in figures such as Figs. 6(b) and S1(b). In this paper, the Pt/SiO_x composite films prepared by the first and second methods are denoted by $Pt_{(epi)}/SiO_x$ and $Pt_{(poly)}/SiO_x$, respectively. Both types of Pt/SiO_x composite prepared on NaCl were then floated on distilled water and mounted on copper grids with a single hole of 0.3 mm^{φ} in their center for photon irradiation experiments and subsequent transmission electron microscopy (TEM) observations. The O content, x, in the SiO_x film was evaluated by X-ray photoelectron spectroscopy to be approximately 1.5 [8].

2.2. Photon irradiation experiments and TEM analysis

The Pt/SiO_x composite films on copper grids were irradiated with photons of energies 680, 140, and 80 eV with beam line BL13 in the Saga Light Source. The diameter of the photon beam was approximately 0.1 mm, and the photon fluxes were estimated to be around 1.8×10^{20}, 5.1×10^{21}, and 3.7×10^{21} photons/(m^2 s) for 680, 140, and 80 eV photons, respectively. The flux usually decreased by about 30% after irradiation for 14.4 ks. The irradiation temperature was room temperature. The copper grid, with the central 0.3 mm^{φ} hole covered with the sample film, was mounted on a holder in the beam line, and the grid position was carefully adjusted by accurately shifting the holder to allow the 0.1 mm^{φ} photon beam to pass through the hole almost at its center. This careful adjustment was made by monitoring the intensity of the photoelectron emission from the copper, i.e., by identifying the grid position at which there was no emission from copper.

This enabled the photon beam to irradiate the sample film at around the center of the 0.3 mm^{φ} hole. These experimental procedures were necessary for subsequent TEM observations of the irradiated sample film, i.e., to enable ex situ, post photon-irradiation TEM studies of the sample. In irradiation of both the $Pt_{(poly)}/SiO_x$ and $Pt_{(epi)}/SiO_x$ composites, the sample was aligned so that the photon beam was always incident to the Pt side (i.e., incident to the other side of the SiO_x film) of the target sample.

In the TEM studies, bright-field images (BFIs), the corresponding selected area electron diffraction (SAED) patterns, and high-resolution electron microscopy (HREM) images were obtained. The electron microscopes used were a 100 kV microscope (Hitachi-H7000) operated at 75 kV and 200 kV microscopes (JEM-ARM200F) operated at 200 kV.

Note that, as a reference, a series of electron irradiation experiments on the same samples were also conducted (see section *3.4*)

3. Results and discussion

3.1. Formation of platinum silicide by irradiation with 680 eV photons

Figure 1 shows an example of silicide formation in the $Pt_{(epi)}/SiO_x$ composite induced by 680 eV photon irradiation for 14.4 ks. Figure 1(a) and 1(b) show a BFI of the composite before irradiation and the corresponding SAED pattern, respectively. Figure 1(a) shows Pt particles of size approximately 10–20 nm, in most cases connected to each other, embedded in an amorphous SiO_x film. The SAED pattern in Fig. 1(b) can be consistently indexed to the [001] diffraction pattern of [001]-oriented face-centered cubic (fcc) Pt particles superposed on the Debye–Scherrer ring pattern of randomly oriented Pt particles and on the halo pattern from the amorphous SiO_x film; however, the intensities

of the last two patterns are too weak to be clearly visible in the photograph. The reason for the strong preferred orientation of Pt along the [001] direction was discussed in the previous paper [8]. Figure 1(c) and 1(d) show a BFI of the composite after photon irradiation and the corresponding SAED pattern, respectively. Comparisons of Fig. 1(a) with Fig. 1(c) and of Fig. 1(b) with Fig. 1(d) show that after irradiation, a set of regularly arranged extra spots, indexed to the 110 reflections of Pt_2Si (strictly speaking, of α-Pt_2Si), appeared in the SAED pattern, albeit of faint intensity [see spots indicated by arrows in Fig. 1(d)], although there were no appreciable differences between the BFIs. The SAED pattern containing the extra spots can be consistently indexed to the [001] diffraction pattern of [001]-oriented Pt_2Si superposed on the [001] diffraction pattern of [001]-oriented fcc Pt particles and on the Debye–Scherrer rings of randomly oriented fcc Pt particles. The reflections from fcc Pt are considered to come from unreacted Pt. Figure 1(e) shows a key diagram of the SAED pattern shown in Fig. 1(d). The presence of 110 reflections in Fig. 1(d) is confirmed by the intensity profile shown in Fig. 1(f); the profile was taken along a line from 000 to $\bar{2}20_{Pt}$ in Fig. 1(d).

Figure 2(a) shows an HREM image of a sample after photon irradiation; the HREM image was taken from the sample a BFI of which is depicted in Fig. 1(c). In the HREM image, areas with a variety of lattice fringes can be observed. In addition to bright areas with salt–pepper contrast only, which probably correspond to amorphous SiO_x, there are areas with right-angled 0.28 nm-spaced lattice fringes (e.g., the framed area A), areas with right-angled 0.20 nm-spaced lattice fringes (e.g., the area indicated by arrow B), and areas with (parallel) 0.20 nm-spaced lattice fringes (e.g., the area indicated by arrow C). An enlargement of area A is shown in Fig. 2(b), with a simulated image (inset). The 0.28 nm-spaced lattice fringes are unique to Pt_2Si and are not expected from fcc Pt, therefore

it is safe to conclude that at least the areas with 0.28 nm-spaced lattice fringes correspond to islands of Pt_2Si that were epitaxially formed on the (001) surface of Pt facing amorphous SiO_x during photon irradiation. This conclusion is consistent with the observation that areas with 0.28 nm-spaced lattice fringes can always be seen in dark regions. All these observations indicate that a platinum silicide, namely Pt_2Si, was successfully formed at the Pt/SiO_x interface in the $Pt_{(epi)}/SiO_x$ composite by irradiation with 680 eV photons.

Silicide formation in the $Pt_{(epi)}/SiO_x$ composite by irradiation with 680 eV photons is consistent with that in the $Pt_{(poly)}/SiO_x$ composite, as shown in Figs. S1 and S2 in the SM [9]. It is concluded that a platinum silicide, Pt_2Si, can be successfully formed in both the $Pt_{(epi)}/SiO_x$ and $Pt_{(poly)}/SiO_x$ composites by irradiation with 680 eV photons.

The effect of electron irradiation during TEM analysis on silicide formation is considered to be negligibly small. For details, see section 1 in the SM [9].

3.2. Formation of platinum silicide by irradiation with 140 eV photons

Figure 3 shows an example of silicide formation in the $Pt_{(epi)}/SiO_x$ composite induced by 140 eV photon irradiation for 14.4 ks. Figure 3(a) and 3(b) show a BFI of the composite before irradiation and the corresponding SAED pattern, respectively. Figure 3(a) shows a continuous thin sheet of Pt, which was formed by sputtering for 50 s, on an amorphous SiO_x film. The SAED pattern in Fig. 3(b) can be consistently indexed to the [001] diffraction pattern of a [001]-oriented fcc Pt sheet superposed on the Debye–Scherrer ring pattern of randomly oriented fcc Pt particles and on the halo pattern from amorphous SiO_x, although the intensities of the last two patterns are too weak to be clearly visible in the photograph. Figure 3(c) and 3(d) show a BFI of the composite after photon

irradiation and the corresponding SAED pattern, respectively. Comparisons of Fig. 3(a) with Fig. 3(c) and of Fig. 3(b) with Fig. 3(d) show that after irradiation a set of regularly arranged extra spots, indexed to the 110 reflections of Pt_2Si, appeared in the SAED pattern, albeit of faint intensity [see spots indicated by arrows in Fig. 3(d)], although there were no appreciable differences between the BFIs. The SAED pattern containing the extra spots can be consistently indexed to the [001] diffraction pattern of [001]-oriented Pt_2Si superposed on the [001] diffraction pattern of a [001]-oriented fcc Pt sheet, if weak patterns such as the Debye–Scherrer ring pattern from randomly oriented Pt particles and the halo pattern from the amorphous SiO_x film are excluded. Figure 3(e) shows a key diagram of the SAED pattern shown in Fig. 3(d). The presence of 110 reflections in Fig. 3(d) is confirmed by the intensity profile shown in Fig. 3(f); the profile was taken along a line from 000 to 220_{Pt} in Fig. 3(d).

Figure 4 shows an HREM image of a sample after photon irradiation; a BFI of this sample is shown in Fig. 3(c). The characteristic features of the HREM image are similar to those of the HREM image in Fig. 2. In the HREM image, there are areas with a variety of lattice fringes, e.g., areas with right-angled 0.28 nm-spaced lattice fringes (e.g., the area encircled in Fig. 4) and areas with (parallel) 0.20 nm-spaced lattice fringes. For the same reasons as those mentioned with reference to Fig. 2, it is concluded that areas such as that with 0.28 nm-spaced lattice fringes correspond to islands of Pt_2Si epitaxially formed on the [001]-oriented Pt particles during photon irradiation. These observations indicate that a platinum silicide, Pt_2Si, can be successfully formed at the Pt/SiO_x interface in the $Pt_{(epi)}/SiO_x$ composite by irradiation with 140 eV photons,.

Silicide formation in the $Pt_{(epi)}/SiO_x$ composite by irradiation with 140 eV photons, shown in Figs. 3 and 4, is consistent with that in the $Pt_{(poly)}/SiO_x$ composite shown in Figs.

S3 and S4 in the SM [9]. It is therefore concluded that a platinum silicide, Pt_2Si, was successfully formed in both the $Pt_{(epi)}/SiO_x$ and $Pt_{(poly)}/SiO_x$ composites by irradiation with 140 eV photons.

Note that the temperature rise of the sample caused by photon irradiation was evaluated to be small. Details are given in section 8 of the SM [9].

3.3. Effects of irradiation with 80 eV photons

Figure 5 shows that a silicide was not formed in the $Pt_{(epi)}/SiO_x$ composite irradiated with 80 eV photons for 14.4 ks. Figure 5(a) and 5(b) show a BFI of the composite before irradiation and the corresponding SAED pattern, respectively. The SAED pattern in Fig. 5(b) can be consistently indexed to the [001] diffraction pattern of [001]-oriented fcc Pt particles superposed on the Debye–Scherrer ring pattern of randomly oriented Pt particles and on the halo pattern from the amorphous SiO_x film, although the intensities of the last two patterns are too weak to be clearly visible in the photograph. Figure 5(c) and 5(d) show a BFI of the composite after photon irradiation and the corresponding SAED pattern, respectively. A comparison of Fig. 5(b) with Fig. 5(d) shows that after irradiation extra spots such as those from the 110 reflections of Pt_2Si did not appear in the SAED pattern. This indicates that a platinum silicide, Pt_2Si, was not formed in the $Pt_{(epi)}/SiO_x$ composite by irradiation with 80 eV photons.

Similarly, silicide formation did not occur in the $Pt_{(poly)}/SiO_x$ composite subjected to irradiation with 80 eV photons, as shown in Fig. S5 in the SM [9]. It is therefore concluded that a platinum silicide, Pt_2Si, was not formed in the $Pt_{(epi)}/SiO_x$ and $Pt_{(poly)}/SiO_x$ composites by irradiation with 80 eV photons.

3.4. Formation of platinum silicide by irradiation with 75 keV electrons, and changes in composition of SiO_x associated with silicide formation

To investigate possible differences between silicide formation by irradiation with photons and electrons, the silicide formation by electron irradiation was examined by in situ TEM. The 100 kV instrument operated at 75 kV and the samples prepared for the photon irradiation experiments were used.

Figure 6 shows an example of silicide formation in the $Pt_{(poly)}/SiO_x$ composite induced by 75 keV electron irradiation. The electron flux, irradiation period, and irradiation temperature were 6.93×10^{22} electrons/(m^2 s), 3.6 ks, and room temperature, respectively. Figure 6(a) and 6(b) show a BFI of the composite before irradiation and the corresponding SAED pattern, respectively. Figure 6(a) shows that Pt particles of size approximately 10 nm, which were mainly isolated from each other, were deposited on an amorphous SiO_x film. The SAED pattern in Fig. 6(b) can be interpreted as the Debye–Scherrer ring pattern of randomly oriented fcc Pt particles superposed on the halo pattern from the amorphous SiO_x film. Figure 6(c) and 6(d) show a BFI of the composite after electron irradiation and the corresponding SAED pattern, respectively. Comparisons of Fig. 6(a) with Fig. 6(c) and of Fig. 6(b) with Fig. 6(d) show that coalescence of particles of heavier (on average) elements (i.e., probably Pt particles with islands of a possible reaction product at the Pt/SiO_x interface) occurred during irradiation, and that a set of extra Debye–Scherrer rings appeared in the SAED pattern after irradiation, although these Debye–Scherrer rings, except for the 110_{Pt2Si} ring, were either too weak in intensity to be clearly visible in the photograph or overlapped with the Debye–Scherrer rings of fcc Pt. The reflections from fcc Pt are considered to come from unreacted Pt. The “hidden” reflections were clearly revealed by intensity profiles obtained by plotting the intensities in the SAED patterns

against the scattering vector, q, taken from Fig. 6(b) and 6(d); the profiles are shown in Fig. 6(e). The bottom profile line, in blue, corresponds to the profile of the SAED pattern for the as-prepared amorphous SiO_x film superposed on the Debye–Scherrer rings from as-prepared fcc Pt particles before irradiation [taken from Fig.6(b)]. The top line, in red, corresponds to the profile for the SAED pattern after irradiation [taken from Fig. 6(d)]. In Fig. 6(e), all the new, apparent peaks in the top profile line can be consistently indexed to reflections from Pt_2Si, indicating successful formation of a silicide, Pt_2Si, in the $Pt_{(poly)}/SiO_x$ composite by electron irradiation. This is fully consistent with silicide formation by electron irradiation in the $Pt_{(epi)}/SiO_x$ composite, shown in Fig. S6 [9], and with that reported in the previous paper [8]. It should be noted on the basis of the SAED patterns (i.e., judged by the intensities of the Pt_2Si reflections), that formation of silicide by electron irradiation was more extensive than in the case of photon irradiation. This point will be further discussed in section *3.5*.

Another point of interest in Fig. 6(e) is that the peak position of the first halo ring from amorphous SiO_x (indicated by a filled triangle) had shifted from a value of $q = 2.60$ nm^{-1} (before irradiation, see the bottom line, in blue) to a value of $q = 2.43$ nm^{-1} (after irradiation, see the top line, in red). These values of q corresponding to the peaks are listed in Table 1, along with the values for amorphous SiO [11] and amorphous SiO_2 [12]. The value of q (i.e., 2.60 nm^{-1}) corresponding to the peak observed on the bottom profile line (in blue) for the as-prepared amorphous SiO_x is small compared with that (i.e., 2.73 nm^{-1}) for amorphous SiO; this seems reasonable because the value of x for the as-prepared amorphous SiO_x is estimated to be larger than 1, i.e., ~1.5 [8]. In contrast, the value of q (i.e., 2.43 nm^{-1}) observed on the top profile line (in red) for amorphous SiO_x after irradiation is close to that (i.e., 2.44 nm^{-1}) for amorphous SiO_2. This suggests that during

electron irradiation, the amount of Si in the amorphous SiO_x in contact with Pt particles became small and eventually reached a level close to that for SiO_2.

To obtain information on the cause of Si depletion in amorphous SiO_x under irradiation, a series of electron irradiation experiments were conducted using as-prepared amorphous SiO_x without any deposited Pt particles. The electron energy and electron flux used were 75 keV and 6.93×10^{22} electrons/(m^2 s), respectively, i.e., the experiments were performed under the same irradiation conditions as those used in the experiments for which the results are shown in Fig. 6. Figure 7 shows an example of the experimental results. Figure 7(a) shows the SAED pattern from the as-prepared SiO_x film, and Fig. 7(b) and 7(c) show those taken after irradiation for 3.6 ks and 7.2 ks, respectively. In Fig. 7(a) through 7(c), the patterns are printed out at two different exposures (shown in left and right halves, respectively) to cover the intensity range as widely as possible. Intensity profiles of the first halo rings in these patterns are shown in Fig. 7(d), as a function of q. Figure 7(d) shows that 75 keV electron irradiation of amorphous SiO_x resulted in slight broadening of the first halo ring but did not bring about a shift in the halo peak position, in contrast to the apparent peak shift seen in Fig. 6(e). This indicates that the Pt particles played an essential role in shifting the peak position during electron irradiation; more specifically, it indicates that Pt particles were necessary for Si depletion of the amorphous SiO_x film during electron irradiation, resulting in an amorphous SiO_x film with a composition close to that of amorphous SiO_2 (see Table 1). The intensity profile of the SAED pattern shown in Fig. S1(d) was compiled to determine whether or not a similar shift of the first halo peak can be induced by photon irradiation. The profile is shown in Fig. 6(e) as a green line (i.e., the middle line). The peak position of the first halo is indicated by a filled triangle, and the corresponding value of q is estimated to be 2.55

nm^{-1} (see Table 1). It is evident that photon irradiation also caused the peak position of the first halo to shift to the low q side and consequently Si depletion occurred in amorphous SiO_x in the $Pt_{(poly)}/SiO_x$ composite film, although the extent of the depletion was small compared with that caused by electron irradiation.

The data shown in Figs. 1 through 6 and in Figs. S1 through S6 indicate that the same silicide, i.e., Pt_2Si, was formed at the Pt/SiO_x interface in both the $Pt_{(epi)}/SiO_x$ and $Pt_{(poly)}/SiO_x$ composites, by either photon or electron irradiation. More specifically, the same silicide was formed by irradiation with 680 or 140 eV photons, or 75 kV electrons. This clearly suggests that silicide formation was induced by electronic excitation under irradiation, and not by knock-on atom-displacements; this is consistent with the suggestion in the previous paper [8].

3.5. Discussion

The experimental results obtained in this work can be summarized as follows.

(1) Silicide formation was successfully induced by irradiation with 680 and 140 eV photons but not by irradiation with 80 eV photons. It was induced also by irradiation with 75 keV electrons.

(2) Depletion of Si occurred in SiO_x in the Pt/SiO_x composite film, in association with silicide formation by both electron and photon irradiation.

3.5.1. Possible mechanism of silicide formation

It is worth discussing the possible mechanism of silicide formation on the basis of summarized result (1) mentioned above, i.e., that silicide formation was successfully induced by irradiation with 680 and 140 eV photons but not by irradiation with 80 eV photons. Figure 8 shows a schematic valence band (VB) diagram for the Si–O binary

system [13], along with the core levels of Si and O atoms. The extent of hybridization between Si orbitals and those of Pt is considered to be small because of the long distance between Si and Pt atoms compared with that between O and Si atoms at the as-prepared Pt/SiO_x interface, therefore it seems reasonable to suppose that the VB at the interface can be conveniently represented by that of the Si–O binary system. Figure 8 and summarized result (1) indicate that excitation of the VB electrons only was insufficient to induce silicidation, and that at least excitation of electrons in the Si2p level, i.e., electrons in the highest-lying Si core level below the VB, was necessary for silicidation to occur. It should also be noted that silicidation was not induced by excitation of Pt4f electrons, of energy 71–74 eV, suggesting that the relevant core-hole Auger decay did not play an essential role in silicide formation. The necessity of excitation of Si2p electrons is similar to the case in the Knotek–Feibleman (K–F) model for O positive ion desorption from the free surface of oxides [14], in which it is envisaged that a core-hole Auger decay mechanism (i.e., Auger decay of a hole in Si2p) is responsible for formation of the O positive ion. In contrast, Tanaka et al. [15] reported that desorption of O positive ions from the free surface of a transition-metal oxide, TiO_2, following metal-core excitation, cannot be fully explained by a mechanism similar to the K–F model, and that a new hypothesis, in which the charge transfer for ion desorption is described by the Kotani–Toyozawa (K–T) model [16,17], explains the experimental results more satisfactorily. However, since no d electrons are present in Si, it is difficult to apply the K–T model directly to the present case. It seems reasonable to suggest that excitation of an electron in the Si2p level at the Pt/SiO_x interface will first bring about a change in the sign of the charge on an O ion (i.e., a change from negative to positive), according to a mechanism similar to the K–F mechanism. This will eventually lead to forced

displacement and removal of the positive O ion from the interface within the solids by repulsive Coulombic interactions with nearby cations, resulting in formation of a bond between Si and Pt at the Pt/SiO_x interface. Such internal displacement of O atoms inside amorphous silicon oxide has been suggested in a paper by Chen et al. [18]. In this way, Si atoms that become free from O atoms, albeit for a short time, can be trapped by Pt atoms at the Pt/SiO_x interface, and repetition of the process can eventually result in formation of a silicide, Pt_2Si, at the Pt/SiO_x interface, accompanied by Si depletion in the matrix of amorphous SiO_x. Such a change in the composition of amorphous SiO_x is consistent with summarized result (2) mentioned beforehand. This may therefore provide a possible framework for the mechanism of silicide formation. A discussion of this mechanism in terms of thermodynamic data available in the literature is given in the SM [9].

3.5.2. Comparison of silicide formation induced by photon irradiation with that induced by electron irradiation

As described in summarized result (1), a platinum silicide, Pt_2Si, was formed at the Pt/SiO_x interface by irradiation with photons (140 eV) or electrons (75 keV). However, SAED patterns suggest that the extent of silicide formation by photon irradiation differs from that by electron irradiation; this can be seen by comparing Fig. 3(d) with Fig. S6(d) and Fig. S3(d) with Fig. 6(d). The characteristic features of the SAED patterns are summarized in Table 2.

We now discuss the difference between silicide formation by photon irradiation (specifically 140 eV photons) and that by electron irradiation (specifically 75 keV electron) in the $Pt_{(epi)}$/SiO_x composite, on the basis of SAED patterns. The SAED pattern

for the $Pt_{(epi)}/SiO_x$ composite after photon irradiation shows four regularly arranged, diffuse, weak spots, which are indexed to the 110_{Pt_2Si} reflections. This SAED pattern can be consistently indexed to the [001] diffraction pattern of [001]-oriented Pt_2Si superposed on the [001] diffraction pattern of [001]-oriented fcc Pt [see Fig. 3(d) and Table 2]. The SAED pattern obtained after electron irradiation, which shows four regularly arranged, sharp, strong spots, which can be indexed to 110_{Pt_2Si} reflections, can be consistently indexed to the [001] diffraction pattern of [001]-oriented Pt_2Si superposed on the [001] diffraction pattern of [001]-oriented fcc Pt [see Fig. S6(d) and Table 2]. These observations suggest that the silicide was formed epitaxially on the Pt surface facing the amorphous SiO_x in the same way for both photon and electron irradiation. The appearance of the sharp and strong 110_{Pt_2Si} spots caused by electron irradiation, in contrast to the diffuse and weak 110_{Pt_2Si} spots from photon irradiation, indicates that silicide formation by electron irradiation was more extensive than that in the case of photon irradiation. The reason for this is discussed in the following. Under the present irradiation conditions, the rate of excitation of Si2p electrons under photon irradiation was slightly higher than that under electron irradiation and the total number of Si2p electrons excited by photon irradiation was about six times greater than the number excited by electron irradiation (see Table S1 in the SM) [9]. If it is assumed that silicide formation is enhanced by increases in parameters such as the rate of excitation of Si2p electrons and the total number of excitations of Si2p electrons, then silicide formation by photon irradiation should be more extensive than that by electron irradiation. However, the experimental results show the reverse. A possible cause of this discrepancy is the differences in the energy levels of the excited electrons. The enhanced silicide formation by electron irradiation can be ascribed to the excitation of electrons in much deeper levels than in the

case for photon irradiation. In 140 eV photon irradiation, excitation of electrons only occurs at energy levels shallower than 140 eV (i.e., if we confine ourselves to electrons in the core levels in Si, only excitation of electrons in the Si2p level occurs), therefore the rate of successful bond formation between Si and Pt will be minimum, leading to limited formation of silicide. In the case of electron irradiation, because excitation of electrons can occur not only at the Si2p core level but also at deeper levels such as Si2s, Si1s, and O1s, resulting in, for example, relaxation via cascade double Auger decay [19], the rate of successful bond formation between Si and Pt will be high, leading to extensive silicide formation.

It seems reasonable to assume that excitation of at least Si2p electrons is necessary for silicide formation but the extent of silicide formation can be influenced by excitation of electrons in deeper levels.

A brief discussion of the difference between silicide formation in the $Pt_{(poly)}/SiO_x$ composite by photon irradiation and that by electron irradiation, based on SAED patterns, is provided in the SM [9].

3.5.3. Atom migration across silicide

It is thought that Si and Pt atom migration across the silicide under irradiation may play an essential role in keeping the Pt concentration at the silicide surface facing the amorphous SiO_x sufficiently high for further trapping of Si by Pt (i.e., for silicide growth) to occur continuously during irradiation. However, details of atom migration are not clear at present. This topic will be the subject of a future study.

3.5.4. Future perspectives

In general, the reaction equilibrium of a solid-state reaction is determined by state variables such as temperature T and the activities of the components, and the direction in which the reaction may proceed is strictly governed by the sign of the change in the Gibbs free energy, ΔG, associated with the reaction [20]. Usually, reversing the sign of ΔG, conventionally by varying the temperature, is difficult. However, the results of the present work show that the synthesis of Pt_2Si at a Pt/SiO_x interface (which is a solid-state reaction that never occurs under simple thermal annealing [8]), can be successfully induced when the system is exposed to an electronic excitation environment. It is worth noting that, in future, direct manipulation of electronic states, such as those used here, could provide a tool for expanding the range of practically possible solid-state reactions, even for inorganic materials.

4. Conclusion

A platinum silicide, Pt_2Si, was successfully formed at a Pt/SiO_x interface by irradiation with 680 and 140 eV photons, but not by irradiation with 80 eV photons. Silicide formation was also induced by irradiation with 75 keV electrons. A larger amount of silicide was formed by electron irradiation than by photon irradiation. Si depletion was observed in amorphous SiO_x in association with silicide formation by both electron and photon irradiation. A possible mechanism of silicide formation by electronic excitation is proposed on the basis of the experimental results.

Acknowledgements

Part of this work was supported by the program Advanced Research Network for Ultra-Microscopic Science (FY2016–), from the Ministry of Education, Culture, Sports,

Science, and Technology (MEXT), Japan. We thank Helen McPherson, PhD, for editing a draft of this manuscript.

References

[1] D. N. Seidman, R. S. Averback, P. R. Okamoto, and A. C. Baily, Amorphization processes in electron- and/or ion-irradiated silicon, Phys. Rev. Lett. 58 (1987) 900-903.

[2] H. Mori, H. Yasuda, T. Sakata, and H. Fujita, Electron-irradiation-induced gold atom implantation into silicon carbide, Radiation Effects and Defects in Solids 124 (1992) 51-59.

[3] S. Takeda and J. Yamasaki, Amorphization in silicon by electron irradiation, Phys. Rev. Lett. 83 (1999) 320-323.

[4] M. T. Winkler, D. Recht, M-J. Sher, A. J. Said, E. Mazur, and M. J. Aziz, Insulator-to-metal transition in sulfur-doped silicon, Phys. Rev. Lett. 106 (2011) 178701.

[5] K. Yasuda, M. Etoh, K. Sawada, T. Yamamoto, K. Yasunaga, S. Matsumura, and N. Ishikawa, Defect formation and accumulation in CeO_2 irradiated with swift heavy ions, Nuclear Instruments and Methods in Physics Research B 314 (2013) 185–190.

[6] S. Takaki, K. Yasuda, T. Yamamoto, S. Matsumura, and N. Ishikawa, Atomic structure of ion tracks in Ceria, Nuclear Instruments and Methods in Physics Research B 326 (2014) 140–144.

[7] H. Yasuda, A. Tanaka, K. Matsumoto, N. Nitta, H. Mori, Formation of porous GaSb compound nanoparticles by electronic-excitation-induced vacancy clustering, Phys. Rev. Lett. 100 (2008) 105506-1–105506-4.

[8] J.-G. Lee, T. Nagase, H. Yasuda, H. Mori, Synthesis of metal silicide at metal/silicon oxide interface by electronic excitation, J. Appl. Phys. 117 (2015) 194307-1–194307-8.

[9] See supplementary material at [http://dx.doi.org/]

[10] G.W. Castellan, Physical Chemistry, second ed., Addison-Wesley Publishing Company, London, 1971.

[11] J.A. Yasaitis, R. Kaplow, Structure of amorphous silicon monoxide, J. Appl. Phys. 43 (1972) 995–1000.

[12] C. Meade, R.J. Hemley, H.K. Mao, High-pressure x-ray diffraction of SiO_2 glass, Phys. Rev. Lett. 69 (1992) 1387–1390.

[13] T.H. DiStefano, D.E. Eastman, Photoemission measurements of the valence levels of amorphous SiO_2, Phys. Rev. Lett. 27 (1971) 1560–1562.

[14] M.L. Knotek, P.J. Feibelman, Ion-desorption by core-hole Auger decay, Phys. Rev. Lett. 40 (1978) 964–967.

[15] S. Tanaka, K. Mase, S. Nagaoka, Photostimulated ion desorption from the TiO_2(110) and ZnO($10\bar{1}0$) surfaces, Surf. Sci. 572 (2004) 43–58.

[16] A. Kotani, Y. Toyozawa, Photoelectron spectra of core electrons in metals with an incomplete shell, J. Phys. Soc. Jpn. 37 (1974) 912–919.

[17] S. Hüfner, Photoelectron Spectroscopy, third ed., Springer, Berlin, 2003, p.114.

[18] G.S. Chen, C.B. Boothroyd, C.J. Humphreys, Electron-beam-induced damage in amorphous SiO_2 and the direct fabrication of silicon nanostructures, Philos. Mag. A78 (1998) 491–506.

[19] Y. Hikosaka, T. Kaneyasu, P. Lablanquie, F. Penent, E. Shigemasa, K. Ito, Multiple Auger decay of the neon 1s-core-hole state studied by multielectron coincidence spectroscopy, Phys. Rev. A 92 (2015) 033413-1–033413-6.

[20] D.R. Gaskell, Introduction to Metallurgical Thermodynamics, second ed., Hemisphere Publishing Corporation, New York, 1981.

Table 1 Peak positions of first halo in intensity profiles of various amorphous (am) silicon oxides. Peak positions of the first halo of amorphous SiO_x in the Pt(poly)/SiO_x composite after 75 keV electron irradiation for 3.6 ks [see the top line, in red, in Fig. 6(e)] and after 680 eV photon irradiation for 14.4 ks [see the middle line, in green, in Fig.6(e)] are included here.

	q (= $2\sin\theta/\lambda$) (nm^{-1})
As-prepared am-SiO_x	2.60
am-SiO_x after 75 keV electron irradiation	2.43
am-SiO_x after 680 eV photon irradiation	2.55
am-SiO [11]	2.73
am-SiO_2 [12]	2.44

Table 2 Comparison of characteristic features of SAED patterns of samples obtained by photon and electron irradiation.

Sample / Quantum	Pt(epi)/SiO_x	Pt(poly)/SiO_x
Photon (specifically 140 eV photons)	SAED shows four diffuse, weak, regularly arranged spots from 110_{Pt_2Si} reflection. The SAED can be indexed to [001] diffraction pattern of [001]-oriented Pt_2Si superposed on [001] diffraction pattern of [001]-oriented fcc Pt [e.g., Fig. 3(d)]	Debye–Scherrer pattern composed of highly segmented rings or, more specifically, of very small number of reflection spots from Pt_2Si [e.g., Fig. S3(d)]
Electron (specifically 75 keV electrons)	SAED shows four sharp, strong, regularly arranged spots from 110_{Pt_2Si} reflection. The SAED can be indexed to [001] diffraction pattern of [001]-oriented Pt_2Si superposed on [001] diffraction pattern of [001]-oriented fcc Pt [e.g., Fig. S6(d)]	Debye–Scherrer pattern composed of normal, continuous rings of reflections from Pt_2Si [e.g., Fig. 6(d)]

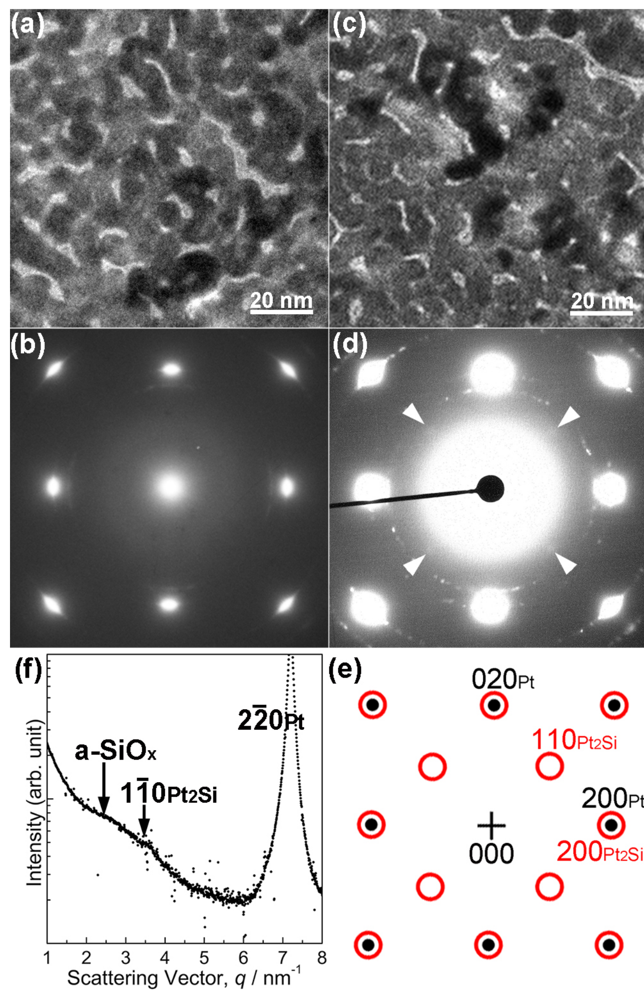

Fig. 1. Silicide formation by photon irradiation of $Pt_{(epi)}/SiO_x$ composite. (a) BFI and (b) SAED pattern before irradiation; (c) BFI and (d) SAED pattern after irradiation; (e) key diagram of pattern in (d); (f) intensity profile taken along line from 000 to $2\bar{2}0_{Pt}$ in (d). Photon energy, flux, and irradiation period were 680 eV, ~1.8×10^{20} photons/(m^2 s) (initial), and 14.4 ks, respectively.

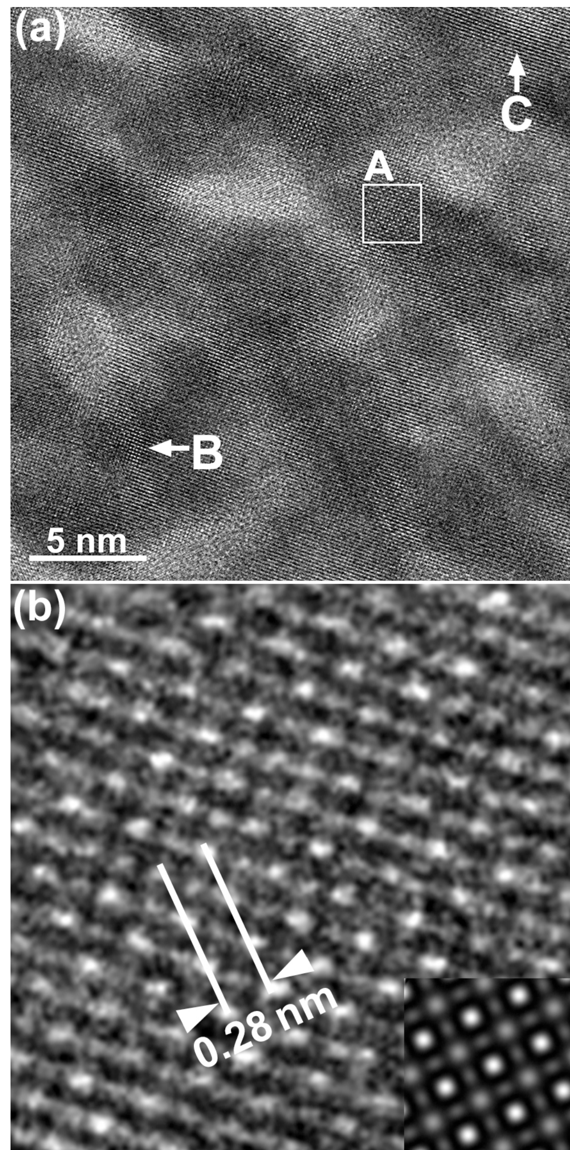

Fig. 2. HREM image of silicide formed by photon irradiation. Photon energy, flux, and irradiation period were 680 eV, ~1.8×10^{20} photons/(m^2 s) (initial), and 14.4 ks, respectively. Sample was the same $Pt_{(epi)}/SiO_x$ composite as was used to obtain images in Fig. 1. (a) HREM image and (b) enlargement of area A in (a) with simulated image (inset). Simulation was performed under the following conditions: 200 kV, Spherical aberration coefficient Cs = 0.5 mm, beam divergence β = 0.5 mrad, thickness t = 8 nm.

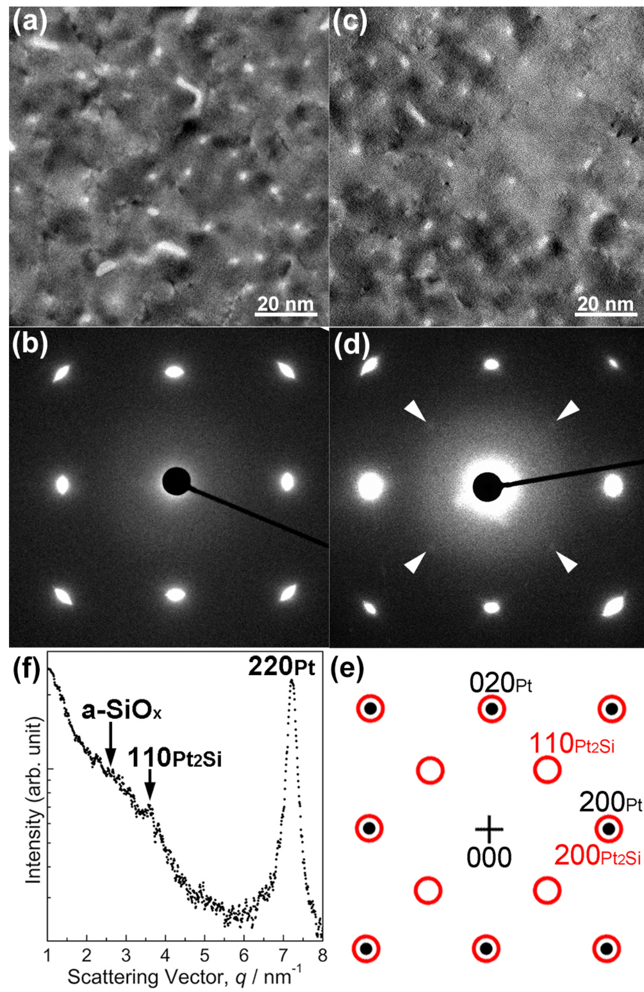

Fig. 3. Silicide formation by photon irradiation of Pt(epi)/SiO_x composite. (a) BFI and (b) SAED pattern before irradiation; (c) BFI and (d) SAED pattern after irradiation; (e) key diagram of pattern in (d); (f) intensity profile taken along line from 000 to 220Pt in (d). Photon energy, flux, and irradiation period were 140 eV, ~5.1 × 10^{21} photons/(m^2 s) (initial), and 14.4 ks, respectively.

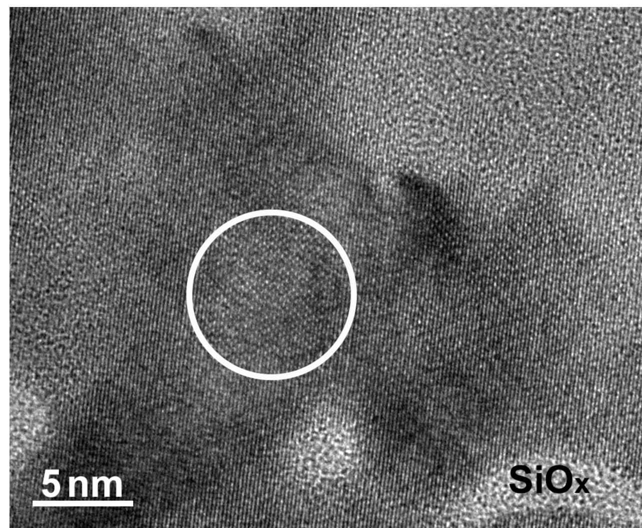

Fig. 4. HREM image of silicide formed by photon irradiation. Photon energy, flux, and irradiation period were 140 eV, ~5.1×10^{21} photons/(m^2 s) (initial), and 14.4 ks, respectively. Sample was the same $Pt_{(epi)}/SiO_x$ composite as that used to obtain images in Fig. 3.

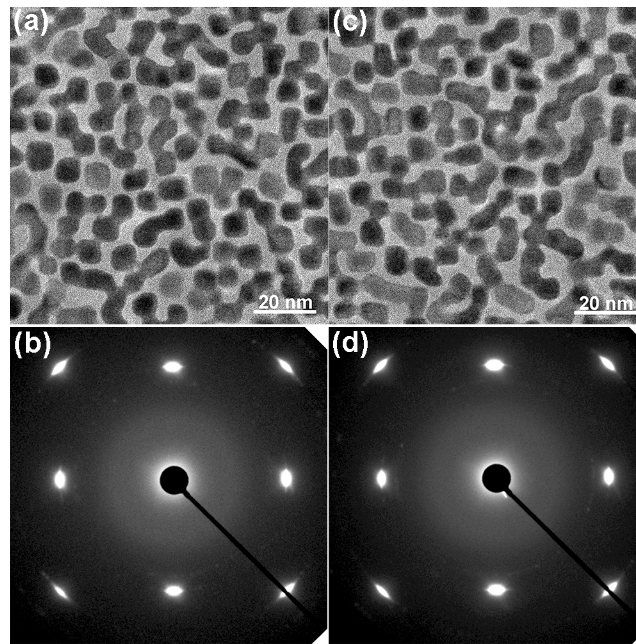

Fig. 5. Absence of silicide formation in $Pt_{(epi)}/SiO_x$ composite under 80 eV photon irradiation. (a) BFI and (b) SAED pattern before irradiation; (c) BFI and (d) SAED pattern after irradiation. Photon flux and irradiation period were ~3.7×10^{21} photons/(m^2 s) (initial) and 14.4 ks, respectively.

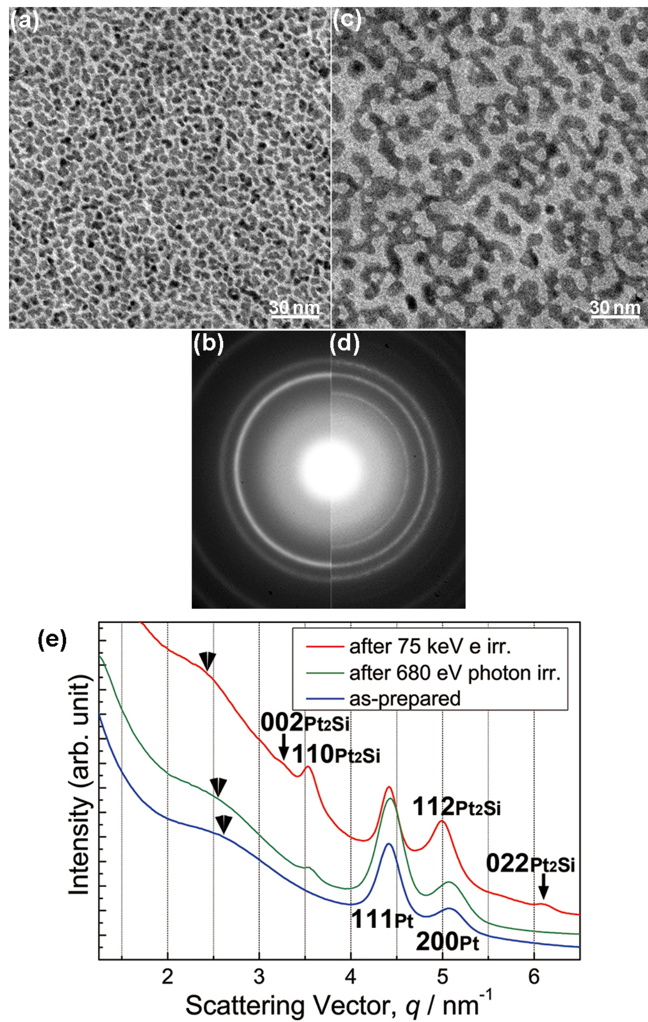

Fig. 6. Silicide formation by electron irradiation of Pt(poly)/SiO_x composite. (a) BFI and (b) SAED pattern before irradiation; (c) BFI and (d) SAED pattern after irradiation. Electron energy, flux, and irradiation period were 75 keV, 6.93×10^{22} electrons/(m^2 s), and 3.6 ks, respectively.

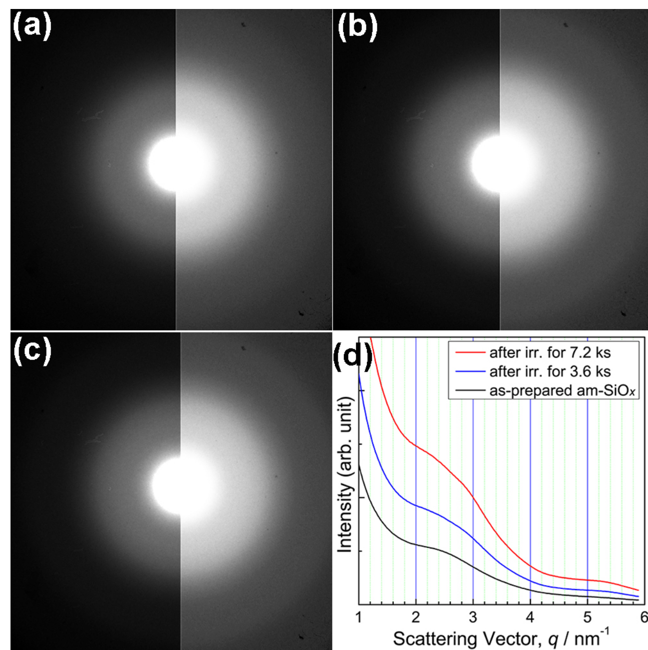

Fig. 7. Electron-irradiation-induced changes in halo pattern of amorphous silicon oxide film without Pt particles. Halo pattern (a) before irradiation; (b) after irradiation for 3.6 ks and (c) 7.2 ks; (d) intensity profiles taken from halo patterns in (a), (b), and (c). Electron energy and electron flux were 75 keV and 6.93×10^{22} electrons/(m^2 s), respectively.

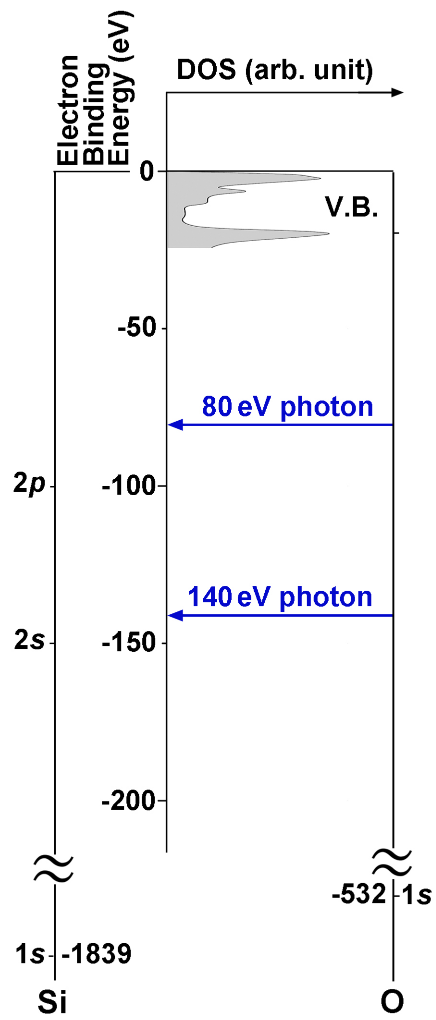

Fig. 8. Schematic diagram of VB of Si–O system, along with relevant core levels of Si and O atoms.

Supplementary Material

Synthesis of platinum silicide at platinum/silicon oxide interface by photon irradiation

K. Sato,[a,b,*] H. Yasuda,[a,b] S. Ichikawa,[a] M. Imamura,[c] K. Takahashi,[c] S. Hata,[d,e] S. Matsumura,[d,f] S. Anada,[g] J.-G. Lee,[h] and H. Mori[a]

[a]*Research Center for Ultra-High Voltage Electron Microscopy, Osaka University, Ibaraki, Osaka 567-0047, Japan*
[b]*Division of Materials and Manufacturing Science, Graduate School of Engineering, Osaka University, Suita, Osaka 565-0871, Japan*
[c]*Synchrotron Light Application Center, Saga University, Honjo 1, Saga 840-8502, Japan*
[d]*The Ultramicroscopy Research Center, Kyushu University, Motooka, Fukuoka 819-0395, Japan*
[e]*Department of Advanced Materials Science and Engineering, 6-1 Kasugakoen, Kasuga-shi, Fukuoka 816-8580, Japan*
[f]*Department of Applied Quantum Physics and Nuclear Engineering, Kyushu University, Motooka, Fukuoka, 819-0395, Japan*
[g]*Japan Fine Ceramics Center, Nanostructures Research Laboratory, Mutsuno, Atsuta, Nagoya 456-8587, Japan*
[h]*Powder & Ceramics Division, Korea Institute of Materials Science, Changwon, Gyeongnam 642-831, Korea*

***E-mail:** sato@uhvem.osaka-u.ac.jp

1. Formation of platinum silicide induced by irradiation of $Pt_{(poly)}/SiO_x$ composite with 680 eV photons

An example of silicide formation in the Pt(poly)/SiO_x composite induced by 680 eV photon irradiation for 14.4 ks is shown in Fig. S1. Figure S1(a) and S1(b) show a BFI of the composite before irradiation and the corresponding SAED pattern, respectively. Figure S1(a) shows that Pt particles of size approximately 10 nm, which in most cases were isolated from each other, were deposited on an amorphous SiO_x film. The SAED pattern in Fig. S1(b) can be interpreted as the Debye–Scherrer ring pattern of randomly oriented fcc Pt particles superposed on the halo pattern from the amorphous SiO_x film. Figure S1(c) and S1(d) show a BFI of the composite after photon irradiation and the corresponding SAED pattern, respectively. Comparisons of Fig. S1(a) with Fig. S1(c) and of Fig. S1(b) with Fig. S1(d) show that a set of extra Debye–Scherrer rings, albeit greatly segmented, appeared in the SAED pattern after irradiation, although there were no appreciable differences between BFIs. The new segmented Debye–Scherrer rings can be consistently indexed to rings of the 002 (arrow 1), 110 (arrow 2), and 112 (arrow 3) reflections of Pt_2Si (strictly speaking, of α-Pt_2Si), as shown in Fig. S1(d). This indicates successful silicide formation in the Pt(poly)/SiO_x composite.

Figure S2(a) shows an HREM image of a sample after photon irradiation; the BFI of the sample is shown in Fig. S1(c). The HREM image is roughly composed of two regions with different degrees of darkness, i.e., one region is bright and the other is dark. In the bright region, the salt–pepper contrast characteristic of an amorphous structure can be seen, therefore the region may correspond to amorphous SiO_x. In the dark region, areas with different lattice fringes can be observed; there are areas with right-angled 0.28 nm-spaced lattice fringes (e.g., the area marked A), areas with (parallel) 0.28 nm-spaced lattice fringes (e.g., the areas marked B and C), and areas with (parallel) 0.2 nm-spaced lattice fringes (e.g., the area marked D). For the same reason as that given in the text with reference to Fig. 2, it seems safe to conclude that at least the areas with 0.28 nm-spaced lattice fringes correspond to islands of Pt_2Si formed during photon irradiation. Figure S2(b) shows a series of simulated HREM images of [001] Pt_2Si. The simulation shows that the right-angled 0.28 nm-spaced lattice fringes observed in area A in Fig. S2(a) are consistent with the simulated images. The observation that areas with the 0.28 nm-spaced lattice fringes can be seen only in the dark region suggests that the platinum silicide was formed at the Pt/SiO_x interface.

The effect of electron irradiation during TEM analysis on silicide formation was considered to be negligibly small. This is because the total dose of electrons during TEM analysis (~1.5×10^{24} electrons/m^2 for 75 keV electrons) was small compared to that necessary to achieve silicide formation solely by electron irradiation (~2.5×10^{26} electrons/m^2 for 75 keV electrons). It is shown in section *3.3* of the main text and in section 3. of the SM that no traces of silicide were detected by TEM analysis when the samples were irradiated with 80 eV photons, indicating a negligible effect of electron irradiation during the TEM analysis.

2. Formation of platinum silicide induced by irradiation of $Pt_{(poly)}/SiO_x$ composite with 140 eV photons

Figure S3 shows an example of silicide formation in the Pt(poly)/SiO_x composite induced by 140 eV photon irradiation for 14.4 ks. Figure S3(a) and S3(b) show a BFI of the composite before irradiation and the corresponding SAED pattern, respectively. Figure S3(a) shows that Pt particles of size approximately 5–10 nm, which in most cases were isolated from each other, were deposited on an amorphous SiO_x film. The SAED pattern in Fig. S3(b) can be interpreted as the Debye–Scherrer ring pattern of randomly oriented fcc Pt particles superposed on the halo pattern from the amorphous SiO_x film. Figure S3(c) and S3(d) show a BFI of the composite after photon irradiation and the corresponding SAED pattern, respectively. Comparisons of Fig. S3(a) with Fig. S3(c) and of Fig. S3(b) with Fig. S3(d) show that some extra, isolated spots appeared in the SAED pattern after irradiation, although there were no appreciable differences between BFIs. The new spots can be consistently indexed to segmented components of the Debye–Scherrer rings of the 110 (indicated by arrow A) and 112 (indicated by arrow B) reflections of Pt_2Si, as shown in Fig. S3(d), although the number of new spots was small. These observations indicate successful silicide formation in the Pt(poly)/SiO_x composite by irradiation with 140 eV photons, although the formation extent was lower than in the case of irradiation with 680 eV photons.

Figure S4 shows an HREM image of a sample after photon irradiation; the BFI of the sample is shown in Fig. S3(c). The HREM image is roughly composed of two regions with different degrees of darkness, i.e., one region is bright and the other is dark. The bright region, which shows salt–pepper contrast, may correspond to an amorphous SiO_x film, as in the case of Fig. 2. In the dark region, areas with different lattice fringes can be observed. It is considered that, of these areas, at least those with 0.28 nm-spaced lattice fringes (e.g., the area marked E in Fig. S4) correspond to islands of Pt_2Si formed during photon irradiation, for the same reason as given with reference to Fig. 2.

3. Absence of silicide formation in Pt(poly)/SiO_x composite irradiated with 80 eV photons

Figure S5 shows the absence of silicide formation in the Pt(poly)/SiO_x composite irradiated with 80 eV photons for 14.4 ks. Figure S5(a) and S5(b) show a BFI of the composite before irradiation and the corresponding SAED pattern, respectively. The SAED pattern in Fig. S5(b) can be consistently indexed to the Debye–Scherrer ring pattern of randomly oriented fcc Pt particles superposed on the halo pattern from amorphous SiO_x. Figure S5(c) and S5(d) show a BFI of the composite after photon irradiation and the corresponding SAED pattern, respectively. A comparison of Fig. S5(b) with Fig. S5(d) shows that after irradiation, no extra reflections from Pt_2Si appeared in the SAED pattern. This indicates that Pt_2Si was not formed in the Pt(poly)/SiO_x composite by irradiation with 80 eV photons.

4. Formation of platinum silicide induced by irradiation of $Pt_{(epi)}/SiO_x$ composite with 75 keV electrons

Figure S6 shows an example of silicide formation in the Pt(epi)/SiO_x composite induced by 75 keV electron irradiation. The electron flux and irradiation period were 6.93 × 10^{22} electrons/(m^2 s) and 3.6 ks, respectively. Figure S6(a) and S6(b) show a BFI of the composite before irradiation and the corresponding SAED pattern, respectively. Figure S6(a) shows that Pt particles of size approximately 10–20 nm, which were mostly connected to each other, were embedded in an amorphous SiO_x film. The SAED pattern in Fig. S6(b) can be consistently indexed to the [001] diffraction pattern of [001]-oriented fcc Pt particles superposed on the Debye–Scherrer ring pattern of randomly oriented Pt particles and on the halo pattern from the amorphous SiO_x film; the intensities of the last two patterns are too weak to be clearly visible in the photograph, as in the cases of Figs. 1(b) and 3(b). Figure S6(c) and S6(d) show a BFI of the composite after electron irradiation and the corresponding SAED pattern, respectively. Comparisons of Fig. S6(a) with Fig. S6(c) and of Fig. S6(b) with Fig. S6(d) show that a set of regularly arranged extra spots, which can be indexed to the 110 reflections of Pt_2Si, appeared in the SAED pattern after irradiation [see Fig. S6(d)], although there were no appreciable differences between the BFIs. The SAED pattern containing the extra spots can be consistently indexed to the [001] diffraction pattern of [001]-oriented Pt_2Si superposed on the [001] diffraction pattern of [001]-oriented fcc Pt particles, and on the Debye–Scherrer rings of randomly oriented Pt particles and the halo pattern from the SiO_x amorphous film, although the intensities of the last two patterns are too weak to be clearly visible in the photograph. Figure S6(e) shows a key diagram of the SAED pattern shown in Fig. S6(d). For an HREM image of a sample after electron irradiation, Fig. 5 in reference [1] should be referred to.

5. Discussion of possible mechanism in terms of thermodynamic data

As described in the introduction in the main text, experiments have confirmed that the present silicide formation does not occur under simple thermal annealing [1]. Here, the experimental results are discussed in terms of thermodynamic data available in the literature. For the Si–O binary system, the following equilibrium reaction is well known and the corresponding thermodynamic data (i.e., the change in the Gibbs free energy, ΔG, associated with the reaction) are available [2,3]:

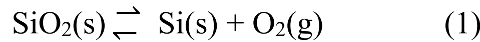

$$SiO_2(s) \rightleftarrows Si(s) + O_2(g) \qquad (1)$$

$$\Delta G = 902\,000 - 174T + RT\ln p_{O_2} \text{ (unit: J)} \qquad (2)$$

where T and p_{O_2} are the temperature and partial pressure of O_2 gas, respectively. Note that in eq. (1), SiO_2 is used instead of SiO_x because silicide formation induced by electronic excitation has been confirmed to occur not only in SiO_x ($x \sim 1.5$) but also in SiO_2 [1]. For the Si–Pt binary system, the following reaction is relevant to the present silicide formation [4]:

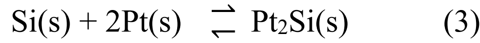

$$Si(s) + 2Pt(s) \rightleftharpoons Pt_2Si(s) \qquad (3)$$

$$\Delta G = -\ 143{,}100 \text{ (in unit of J)} \qquad (4)$$

In eq. (4), ΔG is approximated by the heat of formation of Pt_2Si because the enthalpy change is known to be a good approximation for the free energy change during solid-state compound formation [4].

Summation of eq. (1) through eq. (4) gives

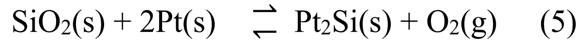

$$SiO_2(s) + 2Pt(s) \rightleftharpoons Pt_2Si(s) + O_2(g) \qquad (5)$$

$$\Delta G = 758\ 900 - 174T + RT\ln p_{O_2} \text{ (unit: J)} \ (6)$$

With T = 298 K and p_{O_2} ~2×10^{-10} atm (which is a rough estimate of the partial pressure of O_2 gas in the electron microscopes used in the study described in reference [1] and in the present study), ΔG in eq. (6) is ~650 kJ. Increasing the temperature to 873 K (i.e., with T = 873 K [1] and po2 ~2×10^{-10} atm) changes ΔG to ~440 kJ. Over the temperature range from 298 to 873 K, ΔG therefore shows large positive values, which means that the reaction described by eq. (5) does not proceed to the right-hand side under conventional thermal annealing conditions. In other words, on the basis of available thermodynamic data, Pt_2Si formation via eq. (5) will never occur under conventional thermal annealing conditions. This thermodynamic-based conclusion is consistent with experimental results (see Fig. 7 in reference [1]). It is therefore confirmed both experimentally and by thermodynamic analysis that silicide (i.e., Pt_2Si) formation will not occur thermally.

In contrast, silicide formation was successfully induced when at least the core electrons at the Si2p level were excited by irradiation with photons or electrons, as described in the main text. If it is assumed that excitation of core electrons enables the reaction described by eq. (1) to proceed to the right-hand side, then such Si atoms, which are now in a reduced state, will spontaneously react with Pt atoms to form Pt_2Si, because ΔG in eq. (4) is always negative, irrespective of temperature. Consequently, it seems reasonable that, of the two constituent reactions, eq. (1) and eq. (3), the reaction described by eq. (1) is directly influenced by electronic excitation, therefore reduction of Si in SiO_2 (or in SiO_x) will take place, and such Si atoms eventually form Pt_2Si, via the reaction in eq. (3), at the Pt/SiO_x interface. This is a thermodynamic explanation of the possible mechanism of silicide formation induced by electronic excitation, which was discussed in section *3.5.1* in the main text.

6. Rate of Si2p excitation and total number of Si2p excitations in photon or electron irradiation

Table S1 lists the rates of Si2p excitation and the total numbers of Si2p excitations in photon or electron irradiation, along with the Si2p excitation cross-sections and quantum fluxes. The last two are necessary to estimate the rate of Si2p excitation and the total number of excitations of Si2p electrons.

7. Brief discussion of difference between silicide formation in $Pt_{(poly)}/SiO_x$ composite by photon irradiation and that by electron irradiation, on basis of SAED patterns

We briefly discuss the difference between silicide formation in the Pt(poly)/SiO_x composite by photon irradiation and that by electron irradiation, on the basis of SAED patterns. The SAED pattern of the composite after photon irradiation is characterized by Debye–Scherrer rings composed of a very small number of reflection spots from Pt_2Si [see Fig. S3(d) and Table 2], whereas that after electron irradiation shows normal, continuous Debye–Scherrer rings of reflection spots from Pt_2Si [see Fig. 6(d) and Table 2]. It is considered that, for the same reason as that given in section *3.5.2* in the case of photon irradiation, the rate of successful bond formation between Si and Pt will be minimum (which would lead to the appearance of highly segmented Debye–Scherrer rings only), whereas, in the case of electron irradiation, the rate will be higher (which would lead to the appearance of normal continuous Debye–Scherrer rings).

8. Temperature rise of sample caused by photon irradiation

Photon irradiation can induce a sample temperature rise, and evaluation of the extent of the rise is of significance in many materials science studies. However, to the best of our knowledge, there are no reports of such studies in the materials science literature, although, in the field of biology, a few theoretical studies have been reported; for example, in one study, possible temperature rises in a model bio-crystal subjected to photon irradiation were investigated and it was reported that the temperature of a thin (100 μm thick) cryo-cooled crystal increased by 6 K under typical irradiation conditions, whereas that of a thick (1000 μm thick) air-cooled crystal increased by 18 K [5]. The experimental conditions used in the present study are different from those assumed in the above calculations, therefore the results indicating temperature rises (i.e., 6 and 18 K) should be regarded only as a guide for rises in the present study.

In this study, it was difficult to measure the temperature rise of the sample directly, for example by using a miniature thermocouple, because the foil sample was too thin (i.e., ~20 nm thick). The extent of the temperature rise was therefore evaluated indirectly, as described below.

When a composite $Pt_{(poly)}/SiO_x$ sample is annealed with no irradiation, grain growth of the Pt particles occurs on the SiO_x substrate, and the magnitude of the grain growth will depend on the temperature; the magnitude of the grain growth can be expressed as a function of temperature. On the basis of this premise, three composite $Pt_{(poly)}/SiO_x$ samples were prepared and annealed for 14.4 ks at 298 (RT), 373, and 573 K, respectively. The results are shown in Fig. S7; Fig. S7(a) and (b) show the as-deposited Pt particles on the substrate and those after annealing for 14.4 ks at 573 K, respectively, and Fig. S7(c) and (d) show the respective corresponding SAED patterns. Fig. S7(e), (f), (g), and (h) show the results after annealing at 373 K, and Fig. S7(i), (j), (k), and (l) show those after annealing at 298 K. All observations were performed with a 200 kV conventional transmission electron microscope. Comparisons of Fig. S7(c) with Fig. S7(d), of Fig. S7(g) with Fig. S7(h), and of Fig. S7(k) with Fig. S7(l) clearly show that no Debye–Scherrer rings from Pt_2Si are observed after annealing at 573, 373, and 298 K, indicating the absence of silicide formation at these annealing temperatures.

The magnitude of the grain growth was evaluated by determining the average radii of

Pt particles on the amorphous SiO_x substrate before ($\overline{r_0}$) and after ($\overline{r}$) annealing at the three temperatures, as follows. The average radius was defined as half of the arithmetical mean of the major and minor axes of the ellipse (i.e., Pt particle). The total counting number was around 200 from each BF image. The average radii obtained are listed in Table S2(A), along with information on the corresponding figures. The average radii of the Pt particles of the sample before ($\overline{r_0}$) and after ($\overline{r}$) 140 eV photon irradiation were also determined and are listed in Table S2(B). The sample subjected to 140 eV photon irradiation was selected because in the 140 eV photon irradiation experiment, the value of the photon energy multiplied by the flux, from which the heat generated in the sample per unit time can be determined, is the highest among those for the present photon irradiation experiments (i.e., 680, 140, and 80 eV photon irradiation experiments). In the present analysis, the value of ($\overline{r} - \overline{r_0}$) was taken as an indicator of the magnitude of the grain growth. The data in Table S2 indicate that the values of ($\overline{r} - \overline{r_0}$) for samples annealed at 298, 373, and 573 K, and for the 140 eV photon irradiation experiment, are 0.0, 0.1, 0.7, and 0.0 nm, respectively. It therefore seems reasonable to consider that grain growth did not occur during annealing at 298 K and in the 140 eV photon irradiation experiment, although detectable grain growth and large, distinct grain growth certainly occurred in the annealing experiments at 373 and 573 K, respectively. These results indicate that the temperature rise of the sample induced by 140 eV photon irradiations is small, and that it is, at most, below 75 K.

On the basis of this analysis, it seems safe to consider that the temperature rise of the sample caused by photon irradiation is small under the irradiation conditions used in this work. In view of this result, the annealing experiment performed at 373 K for 14.4 ks without photon irradiation can be regarded as a marginal control experiment, and provides evidence that silicide formation is not induced by the temperature rise caused by photon irradiation. This evidence is based on the fact that no Debye–Scherrer rings from Pt_2Si were observed after annealing at 373 K for 14.4 ks, as can be seen by comparing Fig. S7(g) with Fig. S7(h)

References for supplementary material

[1] J.-G. Lee, T. Nagase, H. Yasuda, H. Mori, Synthesis of metal silicide at metal/silicon oxide interface by electronic excitation, J. Appl. Phys. 117 (2015) 194307-1–194307-8.

[2] D.R. Gaskell, Introduction to Metallurgical Thermodynamics, second ed., Hemisphere Publishing Corporation, New York, Washington, Philadelphia, London, 1981.

[3] G.W. Castellan, Physical Chemistry, second ed., Addison-Wesley Publishing Company, London, 1971.

[4] R. Pretorius, T.K. Marais, C.C. Theron, Thin film compound phase formation sequence: An effective heat of formation model, Mater. Sci. Eng. Rep. 10 (1993) 1–83.

[5] T. M. Kuzay, M. Kazmierczak, and B. J. Hsieh, X-ray beam/biomaterial thermal interactions in third-generation synchrotron sources, Acta Cryst. D57 (2001) 69-81.

Table S1 Rate of Si2p excitation and total number of Si2p excitations in photon or electron irradiation, and Si2p excitation cross-sections and quantum fluxes.

	Quantum	140 eV photon		75 keV electron	
A	Si2p excitation cross-section (m^2)	5×10^{-22}	[a]	2.4×10^{-23}	[b]
B	Flux ($m^{-2}s^{-1}$)	5.1×10^{21}	[c]	6.9×10^{22}	[c]
C	Rate of Si2p excitation (s^{-1})	~2.6		~1.7	
D	Total number of Si2p excitations	~37 000		~6100	

Note: The rate of Si2p excitation in line C can be obtained by multiplying the cross section in line A by the flux in line B, i.e., C = A × B. In line D, the total number of Si2p excitations during irradiation can be obtained by multiplying the rate of Si2p excitation in line C by the irradiation period, Δt, i.e., D = C × Δt; the values of Δt were 14.4 and 3.6 ks for photon and electron irradiations, respectively. References: [a] J.J. Yeh, I. Lindau, Atomic subshell photoionization cross sections and asymmetry parameters: $1 \leq Z \leq 103$, Atomic Data and Nuclear Data Tables, 32 (1985) 1 - 155; [b] C.J. Powell, Cross sections for ionization of inner-shell electrons by electrons, Rev. Modern Phys. 48 (1976) 33 - 47; [c] Present work.

Table S2. Average radii of Pt particles before ($\bar{r}_0$) and after ($\bar{r}$) annealing at 573, 373, and 298 K are listed in (A). The average radii before ($\bar{r}_0$) and after ($\bar{r}$) 140 eV photon irradiation are listed in (B).

(A)

Annealing temperature (K)	Annealing period (ks)	Average radius of Pt particles after annealing		Average radius of as-deposited Pt particles	
		$\bar{r}$ (nm)	Corresponding figure	$\bar{r}_0$ (nm)	Corresponding figure
573	14.4	3.0 ± 0.8	Fig. S7(b)	2.3 ± 0.6	Fig. S7(a)
373	14.4	2.4 ± 0.7	Fig. S7(f)	2.3 ± 0.6	Fig. S7(e)
298	14.4	2.3 ± 0.8	Fig. S7(j)	2.3 ± 0.8	Fig. S7(i)

(B)

Photon energy (eV)	Irradiation period (ks)	Average radius of Pt particles after irradiation		Average radius of as-deposited Pt particles	
		$\bar{r}$ (nm)	Corresponding figure	$\bar{r}_0$ (nm)	Corresponding figure
140	14.4	3.2 ± 0.6	Fig. S3(c)	3.2 ± 0.6	Fig. S3(a)

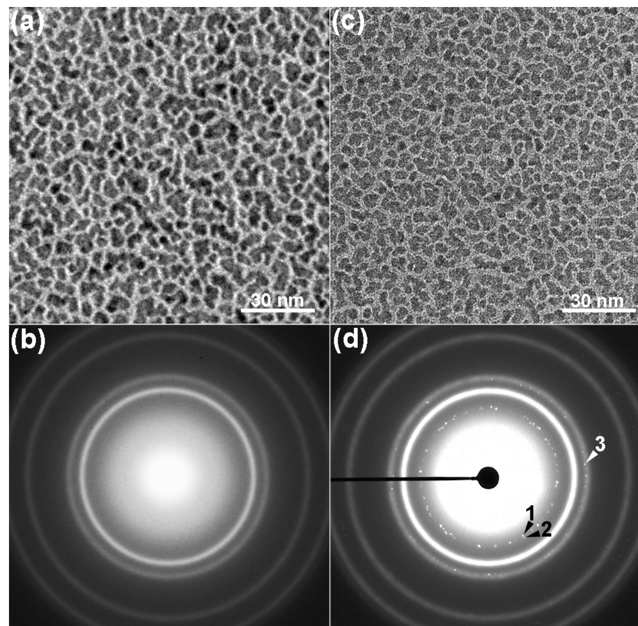

Fig. S1. Silicide formation by photon irradiation of $Pt_{(poly)}/SiO_x$ composite. (a) BFI and (b) SAED pattern before irradiation; (c) BFI and (d) SAED pattern after irradiation. Photon energy, flux, and irradiation period were 680 eV, ~1.8×10^{20} photons/(m^2 s) (initial), and 14.4 ks, respectively.

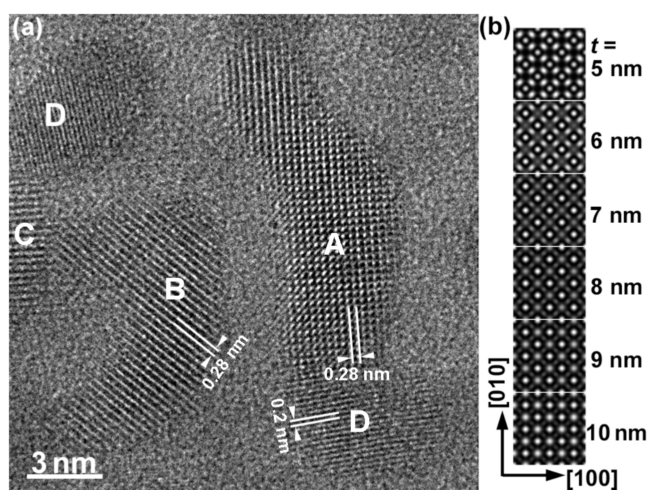

Fig. S2. (a) HREM image of silicide formed by photon irradiation. Photon energy, flux, and irradiation period were 680 eV, ~1.8×10^{20} photons/(m^2 s) (initial), and 14.4 ks, respectively. Sample was the same $Pt_{(poly)}/SiO_x$ composite as that used to obtain images in Fig. S1. (b) Series of simulated HREM images of [001] Pt_2Si.

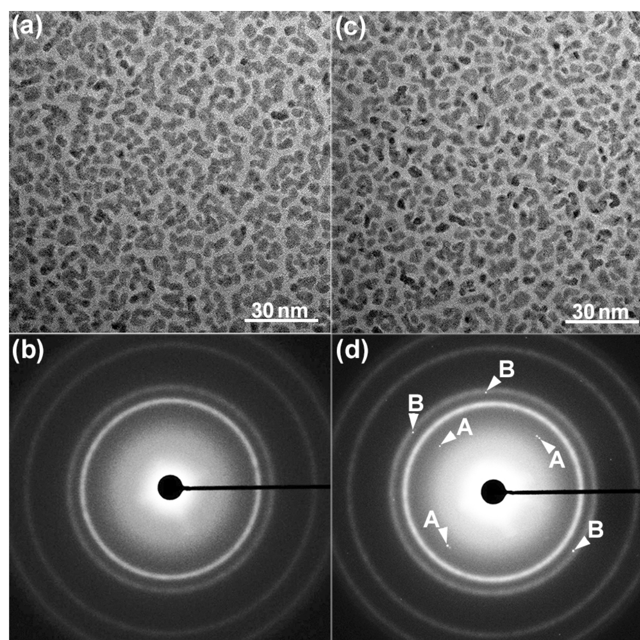

Fig. S3. Silicide formation by photon irradiation of $Pt_{(poly)}/SiO_x$ composite. (a) BFI and (b) SAED pattern before irradiation; (c) BFI and (d) SAED pattern after irradiation. Photon energy, flux, and irradiation period were 140 eV, ~5.1×10^{21} photons/(m^2 s) (initial), and 14.4 ks, respectively.

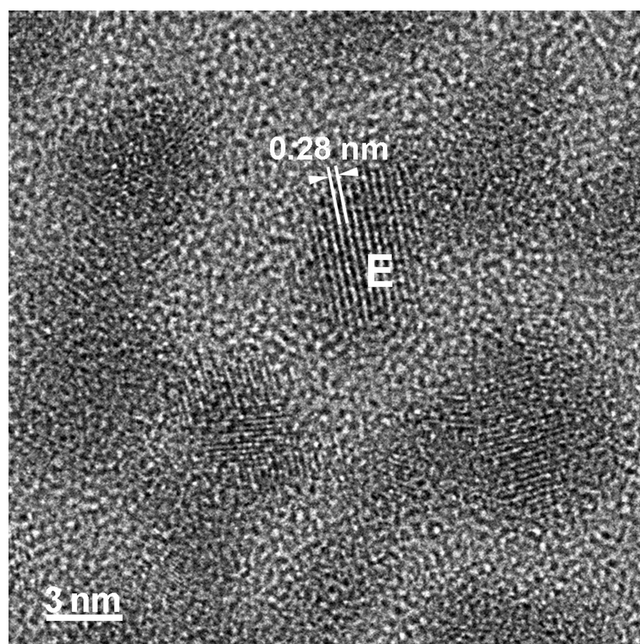

Fig. S4. HREM image of silicide formed by photon irradiation. Photon energy, flux, and irradiation period were 140 eV, ~5.1×10^{21} photons/(m^2 s) (initial), and 14.4 ks, respectively. Sample was the same $Pt_{(poly)}/SiO_x$ composite as that used to obtain images in Fig. S3.

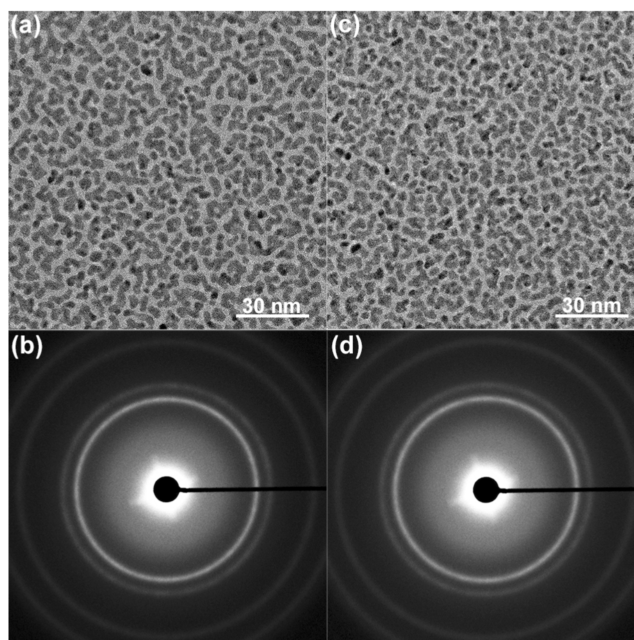

Fig. S5. Absence of silicide formation in $Pt_{(poly)}/SiO_x$ composite under 80 eV photon irradiation. (a) BFI and (b) SAED pattern before irradiation; (c) BFI and (d) SAED pattern after irradiation. Photon flux and irradiation period were ~3.7×10^{21} photons/(m^2 s) (initial) and 14.4 ks, respectively.

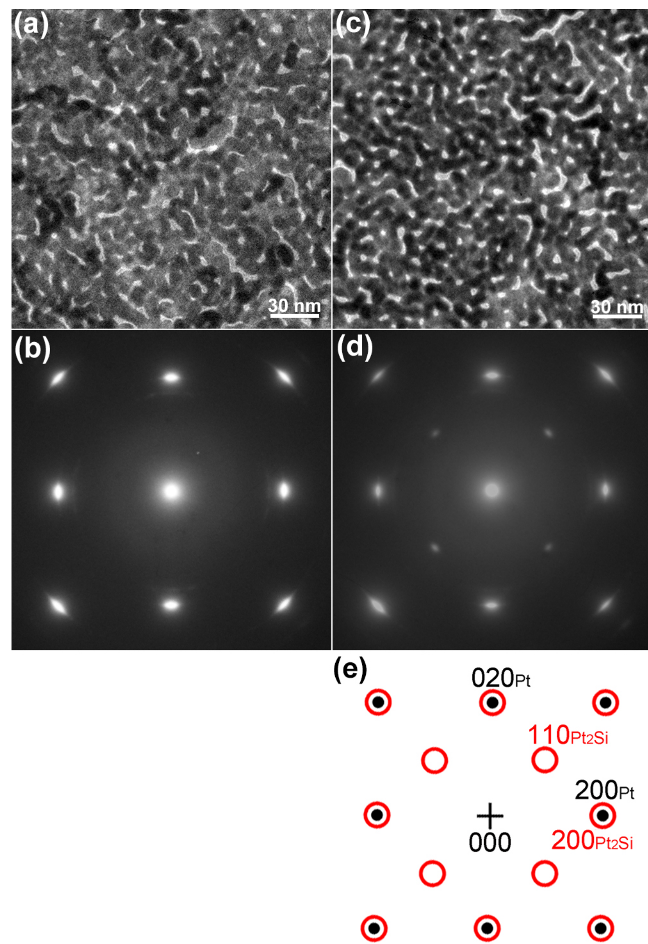

Fig. S6. Silicide formation by electron irradiation of $Pt_{(epi)}/SiO_x$ composite. (a) BFI and (b) SAED pattern before irradiation; (c) BFI and (d) SAED pattern after irradiation; (e) key diagram of pattern in (d). Electron energy, flux, and irradiation period were 75 keV, 6.93×10^{22} electrons/(m^2 s), and 3.6 ks, respectively.

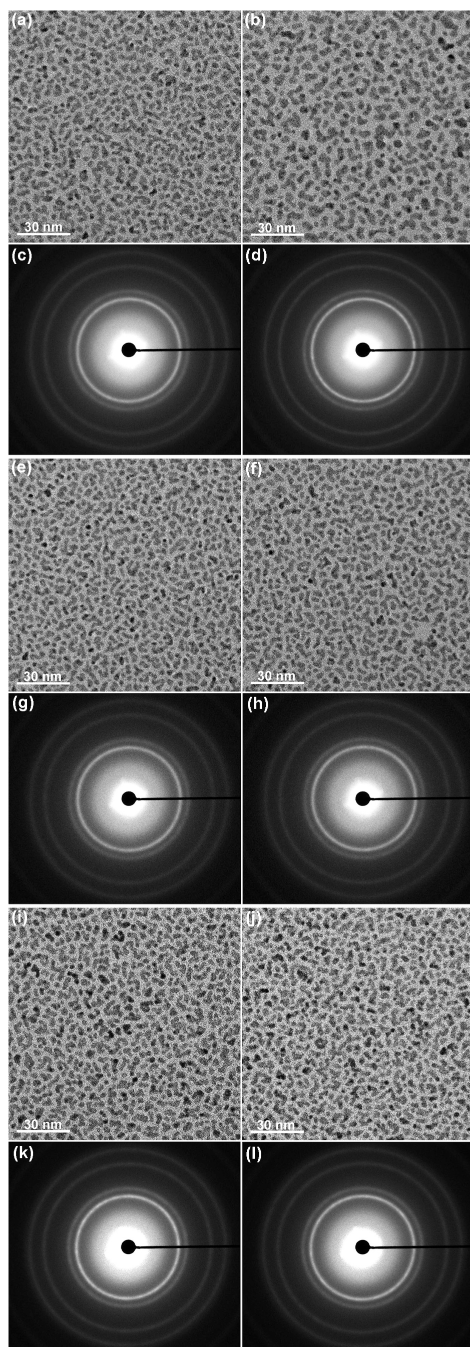

Fig. S7. Grain growth of Pt particles on amorphous SiO_x substrate annealed for 14.4 ks at three different temperatures, without photon irradiation: (a) BFI and (c) SAED pattern before annealing; (b) BFI and (d) SAED pattern after annealing at 573 K; (e) BFI and (g) SAED pattern before annealing; (f) BFI and (h) SAED pattern after annealing at 373 K; (i) BFI and (k) SAED pattern before annealing; (j) BFI and (l) SAED pattern after annealing at 298 K.